A&A 561, A87 (2014)
DOI: 10.1051/0004-6361/201322676

Astronomy & Astrophysics

Terzan 8: a Sagittarius-flavoured globular cluster⋆,⋆⋆,⋆⋆⋆

E. Carretta[1], A. Bragaglia[1], R.G. Gratton[2], V. D'Orazi[3,4], S. Lucatello[2], and A. Sollima[1]

[1] INAF – Osservatorio Astronomico di Bologna, via Ranzani 1, 40127 Bologna, Italy
e-mail: eugenio.carretta@oabo.inaf.it
[2] INAF – Osservatorio Astronomico di Padova, Vicolo dell'Osservatorio 5, 35122 Padova, Italy
[3] Dept. of Physics and Astronomy, Macquarie University, Sydney, NSW 2109, Australia
[4] Monash Centre for Astrophysics, Monash University, School of Mathematical Sciences, Building 28, Clayton VIC 3800, Melbourne, Australia

Received 16 September 2013 / Accepted 6 November 2013

ABSTRACT

Massive globular clusters (GCs) contain at least two generations of stars with slightly different ages and clearly distinct light element abundances. The Na-O anticorrelation is the best studied chemical signature of multiple stellar generations. Instead, low-mass clusters usually appear to be chemically homogeneous. We are investigating low-mass GCs to understand what the lower mass limit is where multiple populations can form, mainly using the Na and O abundance distribution. We used VLT/FLAMES spectra of giants in the low-mass, metal-poor GC Terzan 8 that belongs to the Sagittarius dwarf galaxy to determine abundances of Fe, O, Na, α-, Fe-peak, and neutron-capture elements in six stars observed with UVES and 14 observed with GIRAFFE. The average metallicity is [Fe/H] = -2.27 ± 0.03 (rms = 0.08), based on the six high-resolution UVES spectra. Only one star, observed with GIRAFFE, shows an enhanced abundance of Na and we tentatively assign it to the second generation. In this cluster, unlike what happens in more massive GCs, the second generation seems to represent at most a minority fraction. We discuss the implications of our findings, comparing Terzan 8 with the other Sgr dSph GCs, and to GCs and field stars in the Large Magellanic Cloud, Fornax, and in other dwarfs galaxies.

Key words. stars: abundances – stars: Population II – globular clusters: general – globular clusters: individual: Terzan 8 – stars: atmospheres

1. Introduction

Once considered good examples of simple stellar populations, Galactic globular clusters (GCs) are currently recognised as having formed in a complex chain of events occurring very early in their lifetimes. The fossil record of these events is encrypted in the chemical composition of different stellar populations left over by the process of cluster formation. Exploiting the largest and most homogeneous dataset available to date, Carretta et al. (2010a) showed that most, or perhaps all GCs host multiple stellar populations that can be traced by variations of Na and O abundances. First extensively studied by the Lick-Texas group (see Kraft 1994), these variations are found to be anticorrelated with each other (see e.g. Gratton et al. 2004, 2012, for recent reviews). This notion has been corroborated and extended by photometry, showing that many GCs present spreads or even splits of the evolutionary sequences (see e.g. Lee et al. 2009; Carretta et al. 2011a; Milone et al. 2012a, 2013; Piotto et al. 2012, and references therein). These are attributed to the effect of different chemical composition, in particular of light elements like He, C, N, and O (e.g. Carretta et al. 2011b; Sbordone et al. 2011; Milone et al. 2012a).

Our ongoing FLAMES (Fibre Large Array Multi Element Spectrograph) survey (see Carretta et al. 2006, 2009a,b) allowed for the first time a quantitative estimate of a few relevant parameters. We noted that all GCs analysed have stars of both primordial composition (first generation, FG) and modified composition (second generation, SG), and that the latter are always in the majority (with a ∼30–70% proportion between FG and SG, Carretta et al. 2009a). We also noted that the extension of the Na-O anticorrelation is well correlated to cluster mass (Carretta et al. 2010a). Moreover, there seems to be a sort of observed minimum cluster mass for the appearence of a Na-O anticorrelation, i.e. of a second generation of stars within a cluster. This could be due to a real effect (see Bekki 2011 and also Caloi & D'Antona 2011) or to the lack of statistics available for low-mass clusters. After our survey of more than 20 populous GCs (see e.g. Carretta et al. 2009a,b) we and others are also trying to sistematically sample the border between the lower mass end of the GC population and the higher mass end of old open clusters (see e.g. Bragaglia et al. 2012 and Geisler et al. 2012, and Sect. 5.1). Our intent is to study the chemical composition of a large, representative sample of objects in this mass region in order to give robust contraints to models of cluster formation and evolution.

It is also important to study clusters belonging to other galaxies. A Na-O anticorrelation has been found in old Large Magellanic Cloud (Mucciarelli et al. 2009) and Fornax (Letarte et al. 2006) clusters. However, there are closer GCs of extragalactic origin, namely those of the disrupting Sagittarius dwarf galaxy (Ibata et al. 1994), for which the situation is less clear.

⋆ Based on observations collected at ESO telescopes under programme 087.B-0086
⋆⋆ Tables 2, 3, 7–10 are available in electronic form at http://www.aanda.org
⋆⋆⋆ Full Table 2 is only available at the CDS via anonymous ftp to cdsarc.u-strasbg.fr (130.79.128.5) or via http://cdsarc.u-strasbg.fr/viz-bin/qcat?J/A+A/561/A87

According to Ibata et al. (1995) and Da Costa & Armandroff (1995), at least four GCs appear to be associated with the Sgr dSph, namely M54, Arp 2, Ter 7, and Ter 8. For Law & Majewski (2010), genuine Sgr GCs are Arp 2, M 54, NGC 5634, Ter 8, and Whiting 1, with NGC 5053, Pal 12, and Ter 7 (plus the open cluster Be 29) being likely members; other authors may disagree on the composition of the list, but this is not important for the present paper. Apart from the massive cluster M 54, for which we obtained FLAMES spectra for about 100 stars in the cluster and in the surrounding Sgr field (Carretta et al. 2010b,c), the other Sgr GCs for which chemical abundances based on high-resolution spectroscopy are available are all low-mass GCs. A few stars were analysed in each of them, namely four in Pal 12 (Cohen 2004) with $M_V = -4.48$ (from the Harris 1996 catalogue), five in Ter 7 (Tautvaisiene et al. 2004; Sbordone et al. 2007; $M_V = -5.05$), two in Arp 2 ($M_V = -5.29$), and three in Ter 8 (Mottini et al. 2008; $M_V = -5.05$). No significant spread in proton-capture elements were found. The samples are admittedly small, but these clusters are distant (about 20–30 kpc from the Sun) and even the (often few) stars near the red giant branch (RGB) tip are faint for high-resolution spectroscopy. A possible exception is NGC 4590 (closer to the Sun and for which Fe, Na, and O were presented for more than 40 stars in Carretta et al. 2009a,b), but this cluster is not unanimously assigned to the Sgr family of GCs.

The cluster Ter 8 has been studied by Mottini et al. (2008), together with the other Sgr GC of very low metallicity, Arp 2. They obtained high-resolution spectra using the MIKE spectrograph at the 6.5 m Magellan Telescope, measuring metallicity, α-elements, and heavy elements. Unfortunately, they measured O, but not Na. The abundance of O looks homogeneous in both clusters: [O/Fe] = 0.22[1] (rms = 0.04) dex for Arp 2 and 0.64 (rms = 0.18) dex for Ter 8[2].

Our paper adds six more stars for which the complete set of elements could be obtained, and ten for which at least Fe and Na could be derived; these are nearly all the stars on the RGB brighter than $V = 17$ (see Fig. 1). The paper is organized as follows: our observations are presented in Sect. 2 and the abundance analysis in Sect. 3, while the results are illustrated in Sect. 4. Sections 5 and 6 are devoted to the discussion and to the summary of our findings, respectively.

2. Observations

2.1. Photometry and cluster parameters

We used the V, I photometry published by Montegriffo et al. (1998), kindly provided by the authors, to select our targets. The data were obtained with NTT/EMMI, on a field of view of 9.15×8.6 arcmin^2 and calibrated using a shallower set of data obtained at the 0.9 m CTIO telescope (see Montegriffo et al. 1998 for details). Optical magnitudes were complemented, whenever possible, with K-band magnitudes from the 2MASS Point Source Catalogue (Skrutskie et al. 2006).

The $V, V - I$ colour–magnitude diagram (CMD) of Ter 8 is shown in Fig. 1, with different symbols for the sample of stars observed with FLAMES and according to their radial velocities (RV) measured on our spectra (see below). The tidal radius r_t indicated in the Harris (1996) catalogue is less than 4′, while the half light radius r_h is 0.85′; these values were revised by Salinas et al. (2012) to $r_t = 5.56'$ and $r_h = 2'$. With both sets of values, Ter 8 is a small cluster and it is not easy to select targets for a multi-object spectrograph like FLAMES, which has a field-of-view diameter of 25′. Furthermore, Ter 8 is quite far, at about 26 kpc from the Sun, so only a small fraction of the cluster stars can provide high signal-to-noise (S/N) spectra in reasonable observing times. We selected the targets from the photometry files, after astrometrisation to the GSC-2 systems using programs written by P. Montegriffo at the Bologna Observatory. As in our past works in this project, all the targets are without neighbours; they have no star closer than 3″ (or 2″ but only if at least 2 mag fainter) and were selected because they lie near the RGB (or horizontal branch, HB) ridge line.

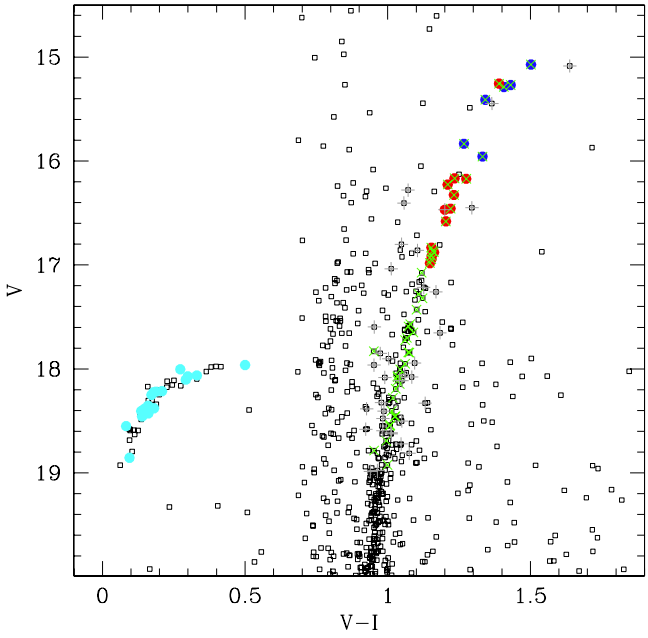

Fig. 1. $V, V - I$ colour–magnitude diagram (CMD) of Terzan 8 from Montegriffo et al. (1998; open symbols). Filled circles indicate the stars in our sample observed with FLAMES/UVES (in blue) and with FLAMES/GIRAFFE (in red) and used for the abundance analysis (with $V < 17$). Filled cyan symbols are HB stars, for which we could not measure the RV. The HB star 1350, at $V - I = 0.5$, is a known RR Lyrae (V2, of type RRc, according to Salinas et al. 2005). Green crosses indicate members on the basis of their RV; grey plus signs are for non members.

2.2. FLAMES data

We obtained exposures with the multi-object spectrograph VLT/FLAMES (Pasquini et al. 2002), as in our previous works on the Na-O anticorrelation (see e.g. Carretta et al. 2009a,b; Bragaglia et al. 2012). The observations were obtained in service mode (see Table 1 for a log). We used the Ultraviolet and Visual Echelle Spectrograph (UVES) 580 nm setup ($\lambda\lambda \simeq$ 4800–6800 Å) and the GIRAFFE high-resolution gratings HR11 (containing the Na I doublet at 5682–5688 Å) and HR13 (which contains the forbidden [O I] line at 6300 Å and the Na I doublet at 6154–6160 Å).

As shown in Fig. 1, we selected seven among the brightest RGB stars for the UVES fibres ($R \simeq 45\,000$). The GIRAFFE fibres (at $R \simeq 24\,200$ for HR11 and 22 500 for HR13) were allocated to fainter objects on or near the RGB or the HB. These

[1] We adopt the usual spectroscopic notation, i.e. $[X] = \log(X)_{star} - \log(X)_{\odot}$ for any abundance quantity X, and $\log \epsilon(X) = \log(N_X/N_H) + 12.0$ for absolute number density abundances.

[2] These values are obtained using Fe II to convert [O/H] to [O/Fe]. As can be seen in Tables 5 and 6 of Mottini et al. (2008), they used Fe II for Arp 2 and Fe I for Ter 8. No relevant difference comes from this choice.

Table 1. Log of the observations.

OB	UT date (Y-M-D)	UT_{init} (h:m:s)	Exp. time (s)	Airmass	Seeing (arcsec)	HR
A	2011-06-24	06:40:15.900	4720	1.018	1.90	11
B	2011-06-24	08:04:10.749	4720	1.106	1.78	11
C	2011-06-28	03:46:57.561	4720	1.159	1.20	11
D	2011-06-28	05:15:05.685	4720	1.029	1.45	11
E	2011-07-04	02:27:08.284	3455	1.346	2.21	11
F	2011-08-27	01:08:41.704	5400	1.037	1.11	11
G	2011-07-22	05:57:38.439	4720	1.079	1.66	13
H	2011-08-27	02:56:06.129	4720	1.034	1.30	13
I	2011-08-28	01:57:43.600	4720	1.013	1.96	13
L	2011-08-28	03:22:55.549	4720	1.066	1.23	13
M	2011-08-30	02:37:19.319	4720	1.028	1.38	13
N	2011-08-31	03:44:36.510	4720	1.121	0.70	13

stars, mostly fainter than $V \simeq 17$, were observed to determine their RV (i.e. their membership status). However, the spectral regions in HR11 and 13 are not ideal for the HB stars, especially at this low metallicity and S/N, and we could not measure their RV. Information on all observed stars can be found in Table 2 (only available at the CDS): ID number; equatorial coordinates; V, I, and 2MASS (Skrutskie et al. 2006) K magnitudes; and the heliocentric RV with its error.

The spectra were reduced (bias and flat-field corrected, 1D extracted, and wavelength calibrated) by the ESO personnel. We applied sky subtraction and division by an observed early-type star (UVES), or a synthetic spectrum (GIRAFFE) to correct for telluric features near the [O I] line using the IRAF[3] routine *telluric*. The latter correction was applied only to the UVES and bright GIRAFFE samples. We shifted all spectra according to the heliocentric velocity and combined the individual exposures; the stars' heliocentric RVs were then measured using *rvidlines* in IRAF. The UVES final spectra have S/N in the range 45–80; the GIRAFFE spectra of stars retained for abundance analysis have median S/N values of 60 and 33 for the HR11 and HR13 spectra, respectively.

The cluster average RV was computed separately for UVES and GIRAFFE spectra, to check possible offsets due to the different resolution and wavelegth calibration. However, we found the same average RV for both samples: $\langle RV_{\rm UVES}\rangle$ = 145.18 (rms = 0.69) km s^{-1} and $\langle RV_{\rm GIRAFFE}\rangle$ = 145.48 (rms = 2.90) km s^{-1}. Figure 2 shows the RV distribution of our stars as a function of distance from the cluster centre and the relative histogram; the cluster's signature is evident in both panels. We considered the objects with RV within 3σ from the mean of the GC as stars in Ter 8. As expected, most of the cluster members are centrally concentrated; the field outliers are found outside about 1 r_c, where the contamination is about 50%.

As a comparison, Harris (1996) has $RV = 130 \pm 8$ km s^{-1}, taken originally from Da Costa & Armandroff (1995), who observed four stars in the IR Ca triplet region at a resolution of about 3 Å, i.e. significantly lower than ours, obtaining individual RVs of 123, 145, 121, and 185 km s^{-1}. Formally, the average of all four is in perfect agreement with our value; the lower value cited in the catalogue is for the three most probable members. Given the very small sample and the lower resolution, their value is in reasonable agreement with ours. We cannot compare our values to Mottini et al. (2008) because they do not provide the RVs for the stars they observed.

[3] IRAF is distributed by the National Optical Astronomical Observatory, which are operated by the Association of Universities for Research in Astronomy, under contract with the National Science Foundation.

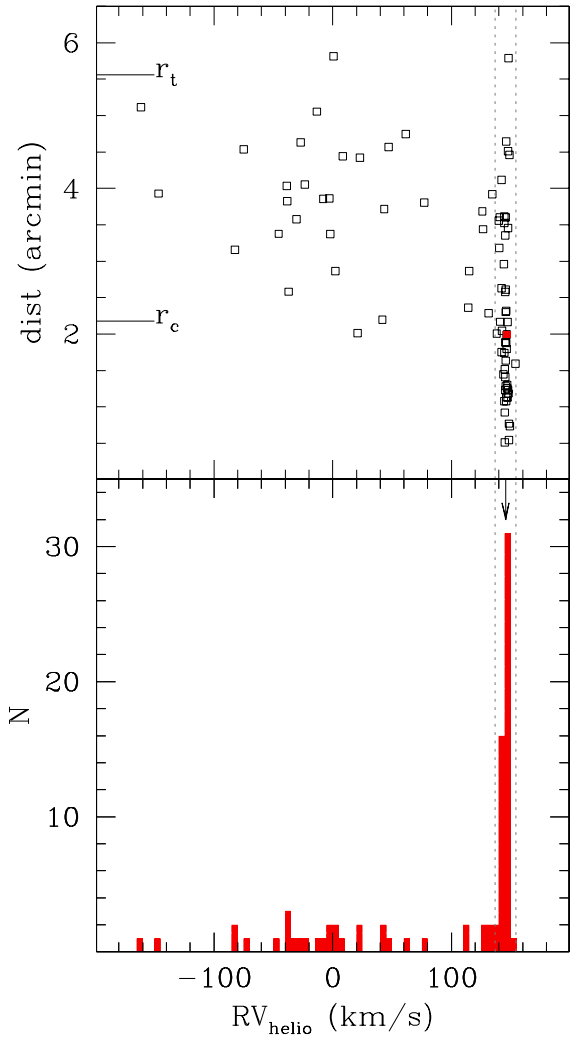

Fig. 2. *Upper panel*: RVs vs. distance from the cluster centre. The core and tidal radii, from Salinas et al. (2012) are indicated. The filled red symbol is the high-Na star 2023 (see text). *Lower panel*: histogram of all RVs for the FLAMES spectra. The arrow indicates the average cluster RV at about 145.5 km s^{-1}. The two vertical lines in both panels indicate $\pm 3\sigma$ from the average.

After pruning the sample using RVs we found a total of 53 member stars (six out of the seven with UVES spectra) and 29 non members out of a total of 101 targets observed. For 19 spectra we could not measure a RV because of the very low S/N and/or the unfavourable wavelength range, as for the HB stars. The individual RV values are given in Table 2; their errors are typically 0.5 and 1.5 km s^{-1} for UVES and GIRAFFE, respectively. Ours is the first measurement of the velocity dispersion in Ter 8; a discussion of the implication of such a small dispersion (2.9 km s^{-1}, for the larger GIRAFFE sample) for the cluster characteristics is deferred to a dedicated paper (Sollima et al., in prep.). Here we would like to note the narrowness of the RGB sequence once the non-members are eliminated (see Fig. 1).

No star noticeably far from the RGB ridge line survived the RV test, except for star 36, which lies slightly to the blue of the RGB. It is at the level expected for the red HB (RHB); however, all the HB is blue in this cluster. Star 36 was not analysed, but

its spectrum does not show any peculiarity (such as, e.g. evident rotation, or evidence of binarity from the RVs). Compared to other stars of similar magnitude, this object looks slightly hotter. It could be a binary with a bluer component (a white dwarf). Emanuele Dalessandro kindly checked the GALEX data (Schiavon et al. 2012) and the star is visible in the near UV, but not on the far UV image, so there is no definitive evidence in favour of a hotter component. This star is included as a member on the basis of its RV, but it is located far from the centre, near the cluster r_t, so it could also be a field interloper. Another interesting possibility is that we have found a post blue straggler star (post-BSS), given its position in the CMD (see Renzini & Fusi Pecci 1988; Fusi Pecci et al. 1992). Some tentative identifications of post-BSS exist (see e.g. Ferraro et al. 1997 for the first evicence of evolved BSS in M 3), and we have found a few other candidates in our studies of the HB (see e.g. Gratton et al. 2013). However, we cannot confirm on the basis of the present data the true nature of star 36. The Ba II 6141 Å line looks slightly more evident than for other stars in Ter 8 of similar atmospheric parameters, and maybe slightly larger, as expected for a post-BSS, but the comparison is difficult, given the low S/N of the spectra.

3. Atmospheric parameters, abundance analysis, and metallicity

We derived the abundances of several elements only for the 16 brightest member stars. The analysis followed as closely as possible the technique used in previous studies by our group concerning the Na-O anticorrelation in GCs (see e.g. Carretta et al. 2006, 2009a,b for extensive references and methods). The main difference was the addition of the Na D lines to avoid having upper limits in Na, because of the combination of low metallicity and S/N. In turn, we were forced to abandon the usual estimates of the microturbulent velocity v_t made by minimizing the slope of the Fe I abundances as a function of the expected line strengths (Magain 1984). The values of v_t obtained with this technique are unsuitable when applied to strong lines such as the Na D or the Ba lines, resulting in strong trends as a function of the microturbulent velocity. The adopted changes in the present abundance analysis are described below.

Line lists, atomic parameters, and reference solar abundances are taken from Gratton et al. (2003). We measured equivalent widths (EW) with the software Rosa (Gratton 1988), as described in Bragaglia et al. (2001). We adopted the same automatic procedure for the definition of the local continuum around each line of previous papers, but we did not correct the GIRAFFE EWs to the UVES system because we did not have any stars observed with both GIRAFFE and UVES.

However, we have two stars in common with those observed by Mottini et al. (2008) in Ter 8 by using the Magellan MIKE spectrograph, with a resolving power of 40 000. Star 1188 (star 305 in Mottini et al.) and star 1209 (star 325 in Mottini et al.) were observed with UVES and GIRAFFE, respectively, in our study. In Fig. 3 we compare our measured EWs with those published by Mottini et al. (2008). The agreement is good in both cases, the average differences (in the sense of our values minus those of Mottini et al.) being $+0.7 \pm 1.2$, $\sigma = 6.9$ mÅ (35 lines) and -3.3 ± 2.0, $\sigma = 7.7$ mÅ (14 lines) for stars 1188 (=305) and 1209 (=325), respectively.

Following the homogeneous approach used in previous papers (see e.g. Carretta et al. 2009a,b) initial temperatures were derived from the $V - K$ colours. We adopted the calibration by Alonso et al. (1999, 2001) for effective temperatures and bolometric corrections. Final temperatures were obtained through a

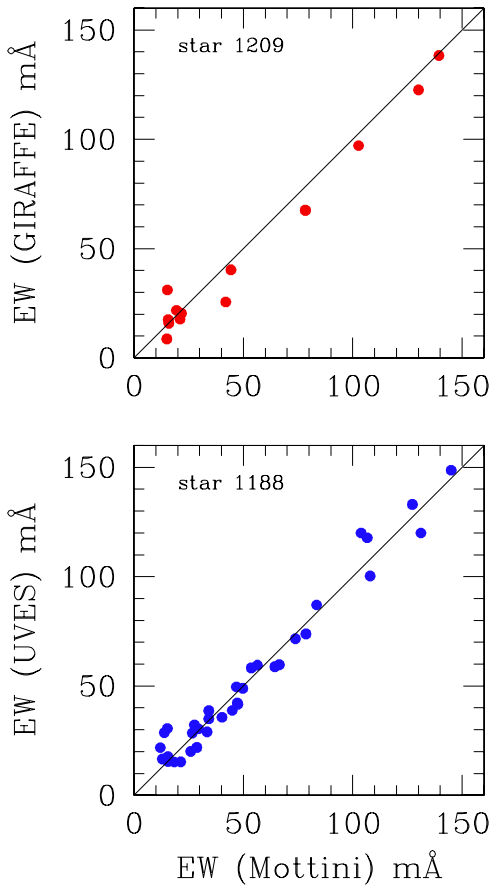

Fig. 3. *Top panel*: comparison of our EWs measured on the GIRAFFE spectrum of star 1209 with those measured by Mottini et al. (2008). *Lower panel*: the same for star 1188; in this case our EWs are measured on the UVES spectrum of the star. In both panels, the solid line is the equality line.

relation with K magnitudes to minimize the star-to-star internal errors. Surface gravities were derived from these temperatures and the position of stars on the CMD, adopting reddening and an apparent distance modulus (0.12 and 17.47 mag) from the web update of the Harris (1996) catalogue. The mass adopted for all stars is 0.85 $M_\odot$ and we used a bolometric magnitude of $M_{bol,\odot} = 4.75$ for the Sun.

At variance with the analysis of previous clusters, for Ter 8 we used the strong Na D lines at 5889.97 Å and 5895.94 Å in addition to the strongest of the two lines at 5682–88 Å, to have Na abundances based on detections, rather than upper limits. Of course, these lines are available only for stars observed with UVES. Furthermore, the abundances derived from strong lines (exceeding 200 mÅ, like the Na D or the Ba II lines) would result in clear trends as a function of v_t, were the values of microturbulence obtained with the usual method employing weaker iron lines. In the present work we then decided to adopt the v_t obtained from the relation as a function of gravity used in Worley et al. (2013) for giants in M 15, a metal-poor GC of similar metallicity.

Maintaining constant temperatures, gravities, and microturbulent velocities, the abundances matching those derived from Fe I lines were interpolated within the Kurucz (1993) grid of model atmospheres (with the option for overshooting turned on) to derive the final abundances. We note that this choice has a minimal impact on the derived abundances with respect to using models with no overshooting. To check this we repeated

Table 4. Sensitivities of abundance ratios to variations in the atmospheric parameters and to errors in the equivalent widths, and errors in abundances for stars in Ter 8 observed with UVES.

Element	Average no. lines	$T_{\rm eff}$ (K)	$\log g$ (dex)	[A/H] (dex)	$v_{\rm t}$ km s^{-1}	EW (dex)	Total internal	Total systematic
Variation		50	0.20	0.10	0.10			
Internal		5	0.04	0.08	0.10	0.10		
Systematic		51	0.06	0.10	0.04			
[Fe/H]I	43	+0.087	−0.025	−0.022	−0.022	+0.016	0.034	0.095
[Fe/H]II	12	−0.022	+0.067	+0.012	−0.014	+0.030	0.037	0.046
[O/Fe]I	1	−0.062	+0.094	+0.040	+0.020	+0.104	0.112	0.072
[Na/Fe]I	3	−0.021	−0.041	+0.027	−0.021	+0.060	0.068	0.061
[Mg/Fe]I	2	−0.036	−0.011	+0.001	+0.002	+0.074	0.074	0.052
[Al/Fe]I	1	−0.046	+0.007	+0.008	+0.022	+0.104	0.107	0.090
[Si/Fe]I	1	−0.067	+0.031	+0.017	+0.021	+0.104	0.107	0.080
[Ca/Fe]I	16	−0.023	−0.004	+0.001	+0.018	+0.026	0.032	0.029
[Sc/Fe]II	7	+0.028	+0.000	+0.004	+0.010	+0.039	0.041	0.035
[Ti/Fe]I	16	+0.027	−0.013	−0.009	+0.005	+0.026	0.028	0.036
[Ti/Fe]II	6	+0.020	−0.012	−0.002	−0.002	+0.042	0.043	0.035
[V/Fe]I	3	+0.021	−0.009	−0.004	+0.020	+0.060	0.063	0.033
[Cr/Fe]I	7	+0.011	−0.013	−0.007	+0.006	+0.039	0.040	0.025
[Cr/Fe]II	2	−0.005	−0.011	−0.008	+0.010	+0.074	0.075	0.039
[Mn/Fe]I	4	+0.004	−0.008	−0.003	+0.016	+0.052	0.054	0.023
[Ni/Fe]I	8	−0.014	+0.008	+0.005	+0.015	+0.037	0.040	0.019
[Cu/Fe]I	1	−0.037	−0.067	+0.004	+0.038	+0.104	0.112	0.055
[Zn/Fe]I	1	−0.097	+0.055	+0.023	+0.015	+0.104	0.108	0.108
[Y/Fe]II	1	+0.122	+0.033	+0.001	+0.038	+0.104	0.112	0.132
[Ba/Fe]II	3	+0.042	−0.037	−0.071	−0.022	+0.060	0.086	0.054
[Nd/Fe]II	3	+0.052	+0.052	+0.004	−0.032	+0.060	0.069	0.142

Table 5. Sensitivities of abundance ratios to variations in the atmospheric parameters and to errors in the equivalent widths, and errors in abundances for stars in Ter 8 observed with GIRAFFE.

Element	Average no. lines	$T_{\rm eff}$ (K)	$\log g$ (dex)	[A/H] (dex)	$v_{\rm t}$ km s^{-1}	EW (dex)	Total internal	Total systematic
Variation		50	0.20	0.10	0.10			
Internal		5	0.04	0.12	0.10	0.14		
Systematic		51	0.06	0.07	0.03			
[Fe/H]I	14	+0.065	−0.014	−0.011	−0.012	+0.038	0.042	0.074
[Fe/H]II	1	−0.017	+0.075	+0.008	−0.004	+0.141	0.142	0.048
[Na/Fe]I	2	−0.039	−0.019	+0.014	+0.010	+0.100	0.102	0.096
[Mg/Fe]I	1	−0.032	+0.003	+0.003	+0.009	+0.141	0.141	0.041
[Si/Fe]I	2	−0.045	+0.020	+0.007	+0.009	+0.100	0.101	0.056
[Ca/Fe]I	4	−0.017	−0.003	−0.001	−0.007	+0.071	0.071	0.031
[Sc/Fe]II	5	−0.051	+0.083	+0.022	+0.008	+0.063	0.071	0.062
[Ti/Fe]I	2	+0.002	−0.003	−0.000	+0.010	+0.100	0.100	0.037
[V/Fe]I	2	+0.012	−0.004	−0.000	+0.011	+0.100	0.100	0.032
[Cr/Fe]I	1	+0.011	−0.003	−0.002	+0.015	+0.141	0.142	0.047
[Ni/Fe]I	2	+0.003	+0.005	+0.002	+0.007	+0.100	0.100	0.021
[Ba/Fe]II	1	−0.041	+0.065	+0.007	−0.069	+0.141	0.158	0.099

the analysis of the six stars observed with UVES using the option with no overshooting, and we found that the effect of this change is negligible. Had we used models with no overshooting we would have obtained [O/Fe] ratios larger by 0.033 dex on average, and [Na/Fe] ratios smaller by 0.007 dex. The remaining element ratios would have changed less than 1 hundredth of dex in most cases. The adopted atmospheric parameters and iron abundances are listed in Table 3 for individual stars.

The details of our procedure to derive errors in the atmospheric parameters are given in Carretta et al. (2009a,b) for UVES and GIRAFFE, respectively. To evaluate the sensitivity of the derived abundances to the adopted atmospheric parameters we repeated our abundance analysis by changing only one atmospheric parameter each time. The amount of the variations in the atmospheric parameters and the resulting variations in abundances of Fe, O, Na, and all elements measured (i.e. the sensitivities) are shown in Tables 4 and 5, for GIRAFFE and UVES spectra, respectively. In the upper part of the same tables we also give the error estimates for each parameter. The typical internal error in $v_{\rm t}$ was evaluated from the rms scatter of the relation between $v_{\rm t}$ and $\log g$ from Worley et al. (2013). The column labelled "total internal" gives the total star-to-star error expected from uncertainties in the atmospheric parameters and in the EWs.

Average abundances for iron and other elements in our sample are listed in Table 6, with those from the study by Mottini et al. (2008) for comparison. Their abundances were corrected to our scale of adopted solar reference abundances (from Gratton et al. 2003). From the analysis of the six stars with high-resolution UVES spectra the mean metallicity we found for Ter 8 is [Fe/H] = −2.271 ± 0.032 ± 0.095 dex (rms = 0.079 dex); the first error bar is from statistics and the second

Table 6. Mean abundances for Ter 8.

Element	no.	avg	rms	no.	avg	rms	no.	avg	rms
		UVES			GIRAFFE			Mottini08	
[O/Fe]I	6	+0.39	0.05				3	+0.52	0.18
[Na/Fe]I	6	+0.25	0.13	10	+0.18	0.27			
[Mg/Fe]I	6	+0.47	0.09	10	+0.46	0.08	3	+0.77	0.21
[Al/Fe]I	6	<0.96	0.19						
[Si/Fe]I	6	+0.25	0.10	8	+0.43	0.09	3	+0.49	0.23
[Ca/Fe]I	6	+0.19	0.04	14	+0.19	0.10	3	+0.40	0.11
[Sc/Fe]II	6	−0.12	0.05	13	−0.01	0.08			
[Ti/Fe]I	6	+0.05	0.06	11	+0.11	0.12	3	+0.07	0.06
[Ti/Fe]II	6	+0.12	0.07				3	+0.16	0.08
[V/Fe]I	6	−0.30	0.06	10	+0.01	0.09			
[Cr/Fe]I	6	−0.41	0.06	3	−0.12	0.08	1	−0.25	
[Mn/Fe]I	6	−0.53	0.05				3	−0.12	0.12
[Fe/H]I	6	−2.27	0.08	14	−2.25	0.12	3	−2.40	0.10
[Fe/H]II	6	−2.27	0.08	5	−2.22	0.09	3	−2.28	0.14
[Ni/Fe]I	6	−0.18	0.03	14	−0.01	0.08	3	−0.09	0.05
[Cu/Fe]I	6	−0.61	0.08				2	−0.82	0.09
[Zn/Fe]I	6	−0.05	0.08						
[Y/Fe]II	6	+0.09	0.09				3	−0.35	0.14
[Ba/Fe]II	6	−0.15	0.08	14	−0.29	0.32	3	−0.15	0.11
[Nd/Fe]II	6	−0.30	0.32				2	+0.03	0.18
[Eu/Fe]II	6	<2.65					3	<1.45	

one refers to the systematic effects. From the larger sample of 14 stars with GIRAFFE spectra we obtained a value of [Fe/H] = −2.249 ± 0.033 ± 0.074 dex (rms = 0.123 dex), in excellent agreement with the estimate from UVES. Compared to the scatter expected from uncertainties in atmospheric parameters and EWs (0.028 ± 0.012 dex for UVES and 0.040 ± 0.011 dex for GIRAFFE) we conclude that in Ter 8 no intrinsic metallicity dispersion statistically different from that predicted from error analysis is present.

The abundances of iron obtained from singly ionized species are in nice agreement with those from neutral lines: [Fe/H]II = −2.28 (rms = 0.08 dex, six stars) from UVES and [Fe/H]II = −2.22 (rms = 0.09 dex, five stars) from GIRAFFE. This supports our adopted atmospheric parameters.

4. Results

4.1. Na and O abundances

The main goal of our study was to determine the Na and O abundances to ascertain whether in this low-mass GC these elements also show an intrinsic star-to-star scatter and an anticorrelation, which is the main spectroscopic signature of multiple populations in GCs.

Corrections for departures from the LTE assumptions to Na abundances were applied following Gratton et al. (1999). Abundances of oxygen were obtained from EWs of the forbidden [O I] 6300.31 Å line measured on spectra cleaned from telluric lines.

In Fig. 4, left panel, we plotted the results from UVES spectra for stars in Ter 8. Apart from a small dispersion in Na, no anticorrelation between Na and O abundances is discernible. From Tables 4 and 6 it is evident that no appreciable intrinsic scatter in the [O/Fe] exists among the six stars in Ter 8 observed with high-resolution UVES spectra. We did not obtain the high average value for [O/Fe] derived by Mottini et al. (2008) from their three stars, nor their large rms scatter (0.18 dex). We do not know the cause of the discrepancy (which is, however, visible in most elements). The solar values for O are about the same (8.76 in their case, 8.79 in ours). The differences in atmospheric

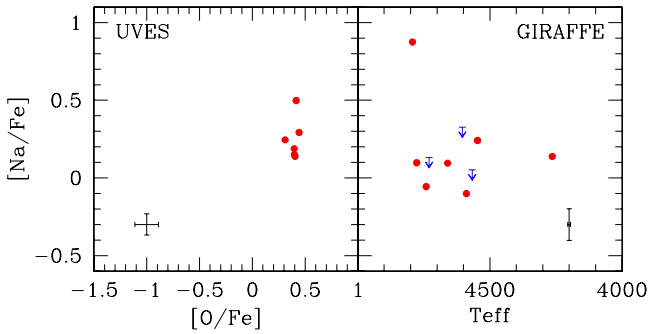

Fig. 4. *Left*: [Na/Fe] ratios as a function of [O/Fe] ratios for stars in Ter 8 with UVES spectra. *Right*: [Na/Fe] as a function of the effective temperature for stars with GIRAFFE spectra. Upper limits in Na are indicated by arrows. In both panels internal error bars are plotted.

parameters for the star 1188 = 305[4] imply a variation of less than +0.1 dex (i.e. in the wrong direction), using the sensitivities of Table 4.

The results we obtained from the GIRAFFE spectra are summarized in the right panel of Fig. 4 as a function of the effective temperature, since no measurement of O lines was possible on these spectra, too noisy in the [O I] region. For Na, we were able to derive seven actual detections and three upper limits.

Stars observed with GIRAFFE have a mean value of [Na/Fe] = +0.18 ± 0.09 with a rms of 0.27 dex. Once the most Na-rich star is excluded from the average, the mean [Na/Fe] ratio becomes 0.10 ± 0.04 dex, while the rms scatter decreases to 0.13 dex, compatible with the star-to-star error (0.10 dex) expected from uncertainties in the abundance analysis. The Na-rich star 2023 has a [Na/Fe] ratio of 0.88 dex, i.e. more than 5σ away from the average value defined by the other nine stars.

In Fig. 5 we show the GIRAFFE spectrum of star 2023 in the region of the Na I doublet at 5682–88 Å, compared to the spectra of the two stars with the most similar atmospheric parameters having Na measurements (one detection and one upper limit). All three objects are among the warmest in our sample, but, despite the less-than-excellent quality of the spectra, it is clear that star 2023 is different from the comparison stars. Using Table 5, it is possible to evaluate that differences in atmospheric parameters should produce a cumulative maximum difference in [Na/Fe] of less than 0.1 dex for both star 1077 and 2124. The actual difference in the Na abundance with respect to star 2023 is much larger than this, so we regard this as a robust detection of an high value of [Na/Fe].

If the high Na content is intrinsic to this star, this object represents the group of second-generation stars in Ter 8. Alternatively, Na-rich material could have been accreted from a companion star; however, the RV of star 2023 is in very good agreement with the cluster average, so it is unlikely that it belongs to a binary system or that it is a field interloper. It would be interesting to study this star further, not an easy task, given its faint magnitude (V = 16.98).

4.2. Other proton-capture elements

Other light elements typically involved in the network of proton-capture reactions at high temperature are Mg, Al, and Si. For aluminum we only obtained upper limits from the only transitions falling in the spectral range of UVES spectra, the doublet

[4] The other star in common, 1209 = 325, was observed with GIRAFFE and we did not derive its oxygen abundance. In this case, the atmospheric parameters are almost identical.

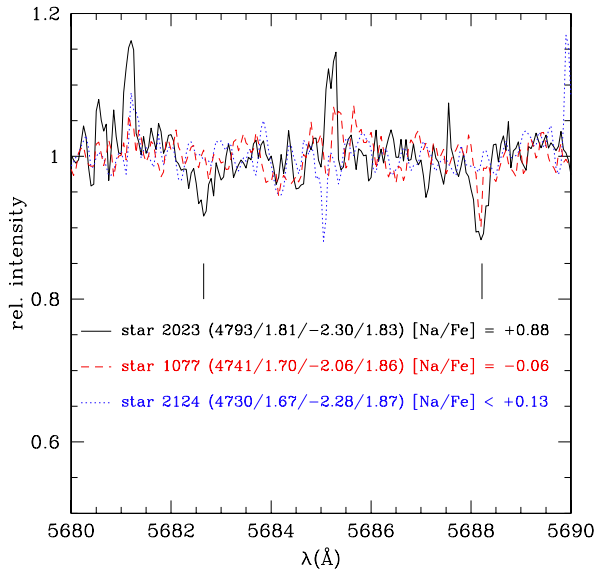

Fig. 5. Portion of the HR11 GIRAFFE spectrum for star 2023 in the region of the Na doublet at 5682.65 and 5688.22 Å (solid black line). The spectra of star 1077 (dashed red line) and of star 2124 (dotted blue line), with the most similar atmospheric parameters in our sample, are superimposed. Sodium abundances for the three stars are labelled.

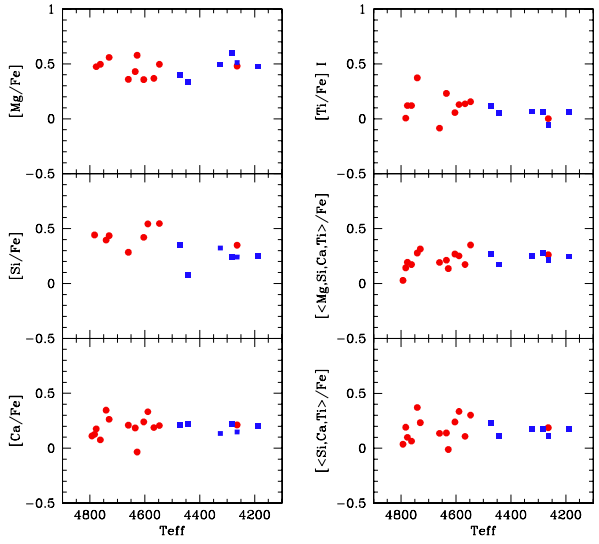

Fig. 6. Abundance ratios of α-elements Mg, Si, Ca, and Ti I as functions of the effective temperature. The average of [α/Fe] ratios are shown in the last two panels on the *right column* (including and excluding the Mg abundance from the mean, respectively). Red circles are for stars observed with GIRAFFE, while blue squares indicate stars with UVES spectra. Internal star-to-star errors are listed in Table 5 and Table 4, respectively.

Al I 6696–98 Å. Abundances of these elements in individual stars are listed in Table 7 and Table 8; mean values obtained from UVES and GIRAFFE spectra are in Table 6.

The run of Mg and Si as a function of the effective temperature is plotted in Fig. 6 for stars with GIRAFFE (red circles) and UVES (blue squares) spectra. Abundances of Mg and Si do not seem anticorrelated with each other, especially when considering the associated error bars. This occurrence points to a simple pre-enrichment by Type II supernovae in the proto-cluster cloud, which was not modified afterwards by hot proton-capture processes (see e.g. Yong et al. 2005; Carretta et al. 2009b, for examples of GCs with clear Si-Mg anticorrelation).

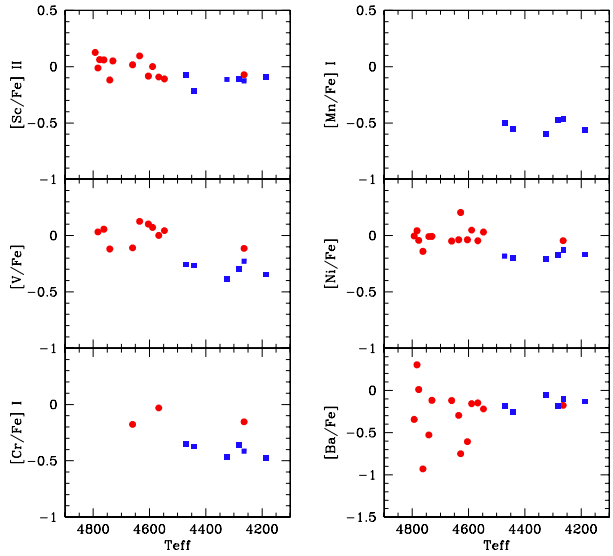

Fig. 7. As in Fig. 6 for elements of the Fe-group (Sc II, V, Cr I, Mn, Ni), and the *s*-process element Ba II.

4.3. Other elements

In addidtion to Mg and Si (potentially involved in proton-capture elements), we measured the abundances of α-elements Ca and Ti. Neither of these elements, in particular Ca, presents any intrinsic scatter or trend as a function of the effective temperature (Fig. 6).

Abundances for elements of the Fe-group Sc II, V I, Cr I, and Ni I were obtained from both GIRAFFE and UVES spectra, and are listed in Table 9. From Fig. 7 there is good agreement between the UVES and the GIRAFFE sample, apart from Cr and V, where an offset seems to be present between the two sets. From the UVES spectra, with larger spectral coverage, we also derived abundances of Cr II, Mn, and Zn. Details on the transitions used in the analysis can be found in Carretta et al. (2011a); information on corrections due to the hyperfine splitting adopted for Sc, V, and Mn are provided in Gratton et al. (2003).

Abundances for Cu, Y, Ba, and Nd (Tables 9 and 10) were derived following the procedure outlined in Carretta et al. (2013). In the present case, because of the much lower metallicity of the cluster under analysis, we could only place upper limits to the Eu abundances.

5. Discussion: stellar generations in Ter 8

A summary of average abundances of several elements in GCs associated with the Sgr dSph is given in Table 11. All these abundances were derived from high-resolution spectra. To these, we added the abundances derived for stars belonging to the Sagittarius nucleus in Carretta et al. (2010c), as a comparison. The abundance ratios for Pal 12, Ter 7, and Arp 2 are corrected to our scale of solar reference abundances.

5.1. Na and O: Terzan 8 in context

The Na-O anticorrelation is one of the most notable tracers of multiple stellar populations in GCs (see Kraft 1994; Gratton et al. 2001; and Carretta et al. 2010a, for summaries about its discovery, meaning, and distribution among GCs). This chemical signature is so widespread among Galactic GCs that it can be assumed to be the distinctive signature of a genuine GC, as the chemical relation established by the complex chain of events leading to the appearance of a GC (Carretta et al. 2010a). The

Table 11. Mean abundances from high-resolution spectra for GCs associated with Sgr.

Element	Ter 8 UVES			M 54 UVES			Sgr UVES			Pal 12 Cohen04			Ter 7 Sbordone07			Arp 2 Mottini08		
	no.	avg	rms	no.	avg	rms	no.	avg	rms	no.	avg	rms	no.	avg	rms	no.	avg	rms
[O/Fe]I	6	+0.39	0.05	7	−0.02	0.47	2	−0.00	0.09	4	+0.02	0.11	4	+0.15	0.06	2	+0.10	0.04
[Na/Fe]I	6	+0.25	0.13	7	+0.33	0.39	2	−0.19	0.27	4	−0.37	0.04	5	−0.16	0.10			
[Mg/Fe]I	6	+0.47	0.09	7	+0.28	0.09	2	+0.09	0.06	3	+0.25	0.01	5	+0.08	0.07	2	+0.53	0.18
[Al/Fe]I	6	<0.96	0.19	6	+0.65	0.62	2	−0.09	0.33				5	−0.11	0.13			
[Si/Fe]I	6	+0.25	0.10	7	+0.36	0.08	2	+0.20	0.10	4	+0.14	0.05	5	+0.10	0.07	2	+0.33	0.01
[Ca/Fe]I	6	+0.19	0.04	7	+0.32	0.08	2	+0.14	0.01	4	−0.08	0.04	5	+0.12	0.13	2	+0.46	0.01
[Sc/Fe]II	6	−0.12	0.05	7	−0.08	0.12	2	−0.22	0.02	4	−0.10	0.04	5	−0.26	0.10			
[Ti/Fe]I	6	+0.05	0.06	7	+0.18	0.10	2	+0.03	0.08	4	−0.09	0.03	5	+0.10	0.07	2	+0.17	0.08
[Ti/Fe]II	6	+0.12	0.07	7	+0.27	0.12	2	+0.08	0.21	4	−0.04	0.05				2	+0.17	0.08
[V/Fe]I	6	−0.30	0.06	7	−0.07	0.09	2	+0.17	0.25	4	−0.31	0.04	5	−0.01	0.10			
[Cr/Fe]I	6	−0.41	0.06	7	+0.06	0.09	2	−0.10	0.03	4	+0.07	0.07	5	−0.01	0.05	2	−0.08	0.06
[Mn/Fe]I	6	−0.53	0.05	7	−0.49	0.09	2	+0.01	0.14	4	−0.21	0.03	3	−0.21	0.07	2	−0.29	0.05
[Fe/H]I	6	−2.27	0.08	7	−1.51	0.16	2	−0.74	0.22	4	−0.82	0.03	5	−0.61	0.06	2	−1.80	0.04
[Fe/H]II	6	−2.27	0.08	7	−1.48	0.17	2	−0.73	0.11	4	−0.66	0.02	5	−0.57	0.05	2	−1.87	0.03
[Co/Fe]I				7	−0.15	0.15	2	−0.29	0.11	4	−0.28	0.04	5	−0.16	0.12	2	−0.12	0.12
[Ni/Fe]I	6	−0.18	0.03	7	−0.09	0.03	2	−0.17	0.07	4	−0.19	0.05	5	−0.20	0.05	2	−0.07	0.14
[Cu/Fe]I	6	−0.61	0.08	7	−0.61	0.18	2	−0.55	0.07	4	−0.51	0.48	3	−0.49	0.20	2	−0.85	0.23
[Zn/Fe]I	6	−0.05	0.08	7	+0.03	0.15	2	−0.14	0.02	3	−0.48	0.13	3	−0.27	0.20			
[Y/Fe]II	6	+0.09	0.09	7	−0.18	0.17	2	+0.09	0.25	3	−0.51	0.13	5	−0.18	0.19	2	−0.16	0.08
[Zr/Fe]I				6	−0.12	0.07	2	−0.43	0.23	4	−0.18	0.06						
[Zr/Fe]II				7	−0.09	0.12	2	−0.08	0.01									
[Ba/Fe]II	6	−0.15	0.08	7	+0.17	0.12	2	+0.38	0.32	4	+0.15	0.01	4	+0.32	0.12	2	+0.15	0.03
[La/Fe]II				7	+0.18	0.17	2	+0.06	0.35	4	+0.10	0.09	5	+0.36	0.13	2	+0.12	0.08
[Nd/Fe]II	5	−0.30	0.32	7	+0.49	0.07	2	+0.63	0.36	3	+0.27	0.06	3	+0.42	0.19	2	−0.03	0.07
[Eu/Fe]II	6	<2.65		7	+0.46	0.08	2	+0.54	0.19	4	+0.55	0.06				2	+0.40	0.11

References. References for the analyses are M 54: Carretta et al. (2010b,c); Sgr: Carretta et al. (2010b,c); Pal 12: Cohen (2004); Ter 7: Sbordone et al. (2007; we do not use Tautvaisiene et al. 2004 since their three stars are in this sample; see the Sbordone et al. paper for comparison among their results); Arp 2: Mottini et al. (2008).

open clusters did not seem to present the same chemical pattern, not even the most massive and old. Two of them, of similar age and mass, have been recently investigated in detail: Berkeley 39 and NGC 6791. The first has a homogeneous composition in all studied elements (Bragaglia et al. 2012); the second shows a bimodal distribution in Na abundance and a small spread in O that may be interpreted as a Na-O anticorrelation (Geisler et al. 2012). We are analysing additional data to further investigate this interesting cluster.

While most of the Milky Way (MW) GCs for which Na and O abundances have been derived show the Na-O anticorrelation (Carretta et al. 2010a), there seem to be a few exceptions, such as Pal 12 (Cohen 2004) and Ter 7 (Tautvaisiene et al. 2004; Sbordone et al. 2005), two clusters with a very low present-day mass which do not show any sign of this relation among the (admittedly small) samples of stars investigated so far. Another case seems to be Rup 106, where Villanova et al. (2013), found no significant variation in Na and O for the nine stars examined. It is more massive than the other two, with a present-day mass larger than that of other GCs showing instead a Na-O anticorrelation (see Fig. 1 in Bragaglia et al. 2012). It would be interesting to study this cluster with a sample larger than the nine stars available today, to reach more definitive conclusions on the presence or absence of a secong generation of star. We note that Rup 106 has a young age and is the only object among these three GCs that is not associated with the Sgr dwarf galaxy.

The definition of a bona fide globular cluster proposed by Carretta et al. (2010a) uses a physical, measurable property of clusters (the presence of a peculiar chemical pattern), instead of rather fuzzy definitions based on age (but not all GCs are old), or metallicity (not all GCs are metal poor), or position in the Galaxy (not all GCs reside in the halo), etc. It is a work-in-progress definition, based on the observations and theoretical models presently available. Cases like Rup 106 (not-so-small mass but no Na-O anticorrelation; see Villanova et al. 2013) should be investigated to understand the reason why this aggregate of stars did not develop different stellar generations with distinct chemistry.

The Na and O abundances of individual stars in GCs found to be related to the Sgr dSph are displayed in Fig. 8. Different symbols indicate different GCs and for a comparison we also plot stars of the Sgr nucleus homogeneously analysed by our group (Carretta et al. 2010c; filled grey triangles). Abundances of stars in Pal 12 and Ter 7 were corrected to our scale of solar abundances (Gratton et al. 2003) using the solar abundances adopted in the original papers (Cohen 2004 and Sbordone et al. 2007, respectively).

From this figure it can appreciated how only the most massive GCs (M 54 = NGC 6715) and NGC 4590 (M68) show the presence of a Na-O anticorrelation among their stars. In particular, M 54, sitting in the nucleus of Sgr, shows this feature both in its metal-poor and metal-rich components (not separated in Fig. 8; see Carretta et al. 2010c). Although they show a difference of almost three orders of magnitude in mass (using the absolute magnitude as proxy of the present-day mass), both M 54 and M 68 do participate in the well-defined relation that links the extension of the Na-O anticorrelation and present-day mass (absolute magnitude) found by Carretta et al. (2010a) in their FLAMES survey (see Carretta et al. 2013 for the most recent version). This evidence suggests that, despite being formed not in the main Galaxy, but instead in one of its dwarf satellites, the most massive GCs associated with Sgr were subject to the same

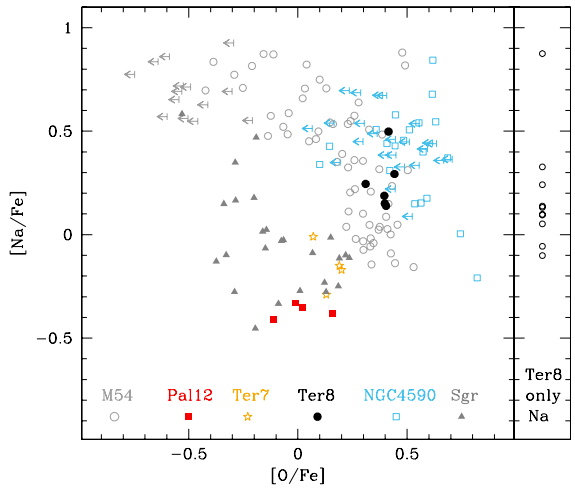

Fig. 8. The Na-O anticorrelation for individual stars in all confirmed Sgr GCs (plus NGC 4590). For Ter 8, we also show the variation in Na for all the stars with GIRAFFE spectra in the *right panel*. In the *left panel*, M 54 (grey empty circles), NGC 4590 (empty squares), and Ter 8 (filled black circles) come from our homogeneous analysis (Carretta et al. 2010c, 2009a,b, and this work, respectively); the abundances of Pal 12 (Cohen 2004, filled red squares) and Ter 7 (Sbordone et al. 2007, open star symbols) have been corrected to our scale of solar abundances (see Gratton et al. 2003). Filled triangles indicate stars of the nucleus of Sgr from Carretta et al. (2010c).

formation mechanism as normal Galactic GCs. The presence of the Na-O anticorrelation, although of different extensions in the two objects, indicates that a first generation must have formed and evolved, and that its most massive members polluted the intracluster gas giving birth to one (or more, as is likely in the case of M 54; Carretta et al. 2010c) additional stellar generation.

The field component of the Sgr dwarf galaxy, represented in Fig. 8 by stars of the nucleus (Carretta et al. 2010c), presents some dispersion in both O and Na. These two elements show no evidence of being anticorrelated with each other in this component. Two stars of the nucleus lie on the lower envelope of the Na-O anticorrelation in M 54 and they can be tentatively assumed to be candidate cluster stars lost to the Sgr nucleus. The few stars studied in Pal 12 (Cohen 2004) and Ter 7 (Sbordone et al. 2007) seem to share the location of stars in the nucleus of Sgr (with which they share the high metallicity) in the Na-O plane. On average, these stars show a slight overabundance of O, with Na about 0.2 dex subsolar (see Table 11; however only the means from the two stars with high-resolution UVES spectra are listed for the Sgr nucleus). They occupy the typical location of Galactic field stars, with high O and low Na abundances. Their position, at lower O values than in the MW ones, is well explained by the longer times involved in the chemical evolution of dwarf spheroidals like Sgr; the higher level of iron, due to the contribution from a relevant number of SN Ia in the enrichment of the intergalactic gas, decreases the [O/Fe] ratio down to solar values (see, however, an alternative scenario in the very recent paper by McWilliam et al. 2013, where the low α-element content is attributed to an initial mass function devoid of the highest mass stars). This explanation is valid also for Pal 12 and Ter 7. Both these GCs are found to be younger than the bulk of the Galactic GCs (see e.g. Carretta et al. 2010a) and also younger than the metal-poor GCs in Sgr (M 54 and M 68). It is likely that stars in Pal 12 and Ter 7 formed from gas already experiencing higher enrichment from Type Ia SNe.

On the other hand, the six giants with UVES spectra in Ter 8 have O and Na abundances compatible with those of M 54 and M 68, and about 0.5 dex higher than the average values observed in Pal 12 and Ter 7. One giant in Ter 8 (not shown in Fig. 8 since it has no O measured) shows a high [Na/Fe] ratio, compatible with a composition modified by proton capture reactions (intermediate component in the classification scheme proposed by Carretta et al. 2009a). If the chemical evolution in Ter 8 was on the verge of developing a Na-O anticorrelation, this may have some impact on the theories illustrating the GC formation. Ter 8 has a present-day mass very similar to that of Ter 7, but the second is more metal rich. The implication is that in addition to the total mass the metal abundance is also a crucial factor: at the same mass, a lower metallicity is favoured for building up a second generation within a cluster. In the best (closest) example of a dwarf spheroidal galaxy with its own system of GCs available to us, it seems that two stellar generations have appeared only amongst the most metal-poor objects.

5.2. Is Ter 8 an FG-only or a mainly-FG cluster?

Caloi & D'Antona (2011) presented a list of candidate GCs only (or mainly) composed of FG stars (Ter 8 and Arp 2 are among them). They based their selection on the possibility of producing the observed HBs with almost a single mass value. This occurrence would indicate the absence of any significant spread in He, and therefore of SG stars. The difference between the two categories proposed by Caloi and D'Antona is that FG-only GCs were not massive enough to retain the gas necessary to form a SG, while mainly-FG clusters could form a SG but did not lose the vast majority of their primordial stars (SG stars are currently supposed to be the majority only because most of the FG was lost by the clusters; see e.g. D'Ercole et al. 2008).

In the present paper we find that there are some Na variations in Ter 8, but the fraction of Na-rich stars is much lower than for most of the GCs studied to date. This is evidence of stars with mostly primordial composition. Only a few objects may be part of a SG, the opposite of what we find for more massive GCs. The binomial distribution is the best way to approach the issue statistically, since one star could belong either to the first or to the second generation. Using this distribution, finding only one SG star out of 16 that were analysed means, that we can exclude the notion that SG stars represent more than 30% of this cluster with a 98% probability, and that they represent more than 15% with a 95% probability.

Considering together the three low-mass Sgr GCs (Pal 12, Ter 7, and Ter 8), we have one bona fide SG star out of 25 (zero out of four and five, respectively, in Ter 7 and Pal 12). Using again the binomial distribution, this would imply that the probability that SG stars represent more than 30% is tiny (about 0.1%). Can we conclude that all the Sgr GCs are examples of FG-only or mainly-FG clusters? As discussed above, the obvious counterexample is M 54, which has one of the most extended Na-O anticorrelations found so far (Carretta et al. 2010b,c). However, this is a very massive GC. Another possible exception is NGC 4590 (M 68; see the previous subsection), although we note that its attribution to the Sgr system of GCs is still disputed (see e.g. Dalessandro et al. 2012). The observed Na-O anticorrelation in this GC is not very extended and this cluster shows one of the highest fractions of FG stars in our FLAMES survey, about 40%.

We can also look at clusters in other dwarf galaxies. The only two cases where detailed abundance analyses of individual giant stars were measured are the dwarf spheroidal Fornax (Fnx) and the dwarf irregular Large Magellanic Cloud (LMC). Letarte et al. (2006) measured nine stars in three GCs of Fnx, Fornax 1, 2, and 3, with total absolute magnitudes $M_V = -5.32, -7.03,$

and −7.66, respectively (van den Bergh & Mackey 2004). These GCs are all very metal poor, with [Fe/H] about −2.3 (Letarte et al. 2006). Only two of the nine analysed stars are classified SG. One star is in Fornax 1, whose M_V is similar to the one in Ter 8 ($M_V = -5.07$ in the Harris 1996 catalogue and −5.68 in Salinas et al. 2012). The second star is in Fornax 3, which has a much larger mass. Taken at face value, this means a fraction of about 20% of SG. On the other hand, D'Antona et al. (2013) analysed the HB of the Fornax clusters. They found no evidence of a second generation in Fornax 1 ($M_V = -5.2$, Webbink 1985) while according to their analysis the remaining brighter clusters ($-8.2 < M_V < -7.2$) should contain 50% or more second-generation stars. The real fraction of second generation stars in these clusters is therefore controversial.

Moving to the LMC, Mucciarelli et al. (2009) found a Na-O anticorrelation in three metal-poor ([Fe/H] ∼ −1.8), massive ($M_V = -7.25, -7.51, -7.70$; van den Bergh & Mackey 2004), old clusters. In this case, however, the proportion between FG and SG among the 18 stars analysed is the same as for the massive MW GCs. Maybe this occurrence is due to the different kind of galaxy (dwarf irregular vs. spheroidal) but we do not have enough data to draw firm conclusions. No spread in Na and O was found in younger and slightly less massive LMC clusters (Mucciarelli et al. 2008). Instead, Johnson et al. (2006) found no significant variation in Na and O among ten stars they analysed in four old LMC GCs, even if they were massive (M_V from −7.40 to −7.75; van den Bergh & Mackey 2004). Johnson et al., however, found a large enhancement in Al in one of the stars, while Hill et al. (2000) measuread a large Al spread in three stars of another LMC cluster. This evidence is rather puzzling, because the temperatures required for the efficient action of the Mg-Al cycle are much higher than those necessary for the activation of the CNO and Ne-Na cycles. The situation for the LMC clusters is still unclear and needs to be studied further using larger and more homogeneous samples.

In N-body simulations built to represent scenarios of GC formation where the main polluters are intermediate mass asymptotic giant branch (AGB) stars (D'Ercole et al. 2008) or fast rotating massive stars (Decressin et al. 2010), a common feature is that the final product (the currently observed cluster) should be more compact than its progenitor (Vesperini et al. 2013). This naturally follows either from the cooling flow collecting gas for the SG in the cluster centre (the D'Ercole et al. scenario) or from the birth or migration of very massive stars to the centre (the Decressin et al. scenario). Taken with the other characteristics of FG stars, this prediction has some consequences for GCs expected to be almost entirely composed of or dominated by FG stars. Among them we should expect i) no spread at all in Na and O (or a very small one); ii) no large spread in He, and therefore a shorter HB compared to GCs of similar mass and metallicity; and iii) a lower concentration. In turn, the last property implies a larger fraction of primordial binaries and a population of blue stragglers and millisecond pulsars more similar to that found in the Galactic field.

Do GCs belonging to dSph galaxies share these peculiarities? As discussed above, even when massive enough, GCs in Sgr and Fnx show a tendency to homogeneous values of Na and O, at least for most of their stellar populations. The situation is less clear for LMC clusters.

The dominance of FG over SG implies a smaller average He content and a smaller dispersion of He abundance. This shows up very well on the HB, whose extension is related to metallicity, age, and He (see e.g. Gratton et al. 2010 and references therein). Gratton et al. determined the dispersion in mass

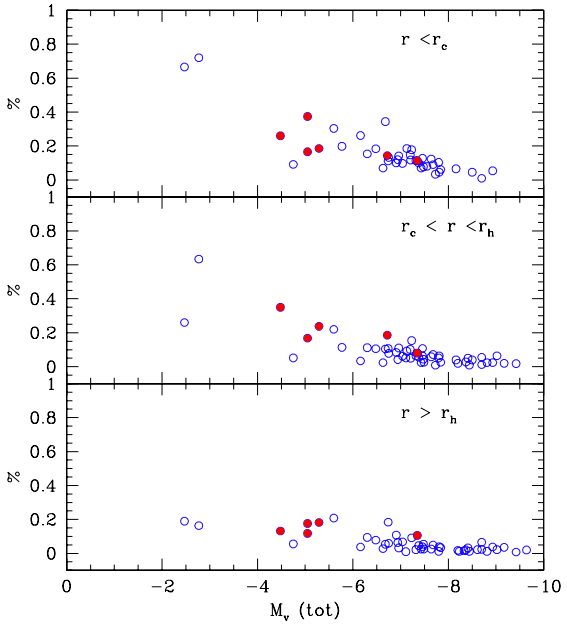

Fig. 9. Total fraction of binaries measured in GCs by Milone et al. (2012b) for their r_c, r_c-HM (where HM indicates the half-mass radius r_h), and oHM samples (*from top to bottom*, respectively; see the original paper for definitions) as a function of the total absolute V magnitude. Filled red symbols indicate the GCs associated with the Sgr dSph (see text).

(i.e. in He, since higher He means lower mass on the HB) in a large number of GCs from their HBs. Unfortunately, only three of the GCs that are probable members of Sgr were studied: NGC 4590, NGC 5053, and NGC 5466. All three GCs have a very low metallicity ([Fe/H]∼ −2.3 dex) and all seem to present a smaller spread in mass for their metallicity, lying clearly below the best-fit line in the mass loss vs. [Fe/H] plane. In the work on UV properties of GCs observed with the GALEX satellite (Dalessandro et al. 2012) the four most metal-poor GCs associated with Sgr (the three mentioned above and Ter 8) are clearly seen separated from the bulk of MW GCs in the $(FUV - V)$ vs. [Fe/H] plane, with Sgr clusters having systematically redder colours than their Galactic counterparts of similar metallicity. Again, this difference can be consistently explained by the different distribution of stars along the HB for MW and Sgr clusters of similar metallicity and age. Dalessandro et al. (2012) found that the average R'-parameter (relating the number of HB and RGB stars) as measured by Gratton et al. (2010) is smaller for the Sgr clusters than for the MW clusters, possibly implying a lower He abundance. This points again towards a dominance of FG stars, since the SG tend to have higher He, and, as a result, brighter and bluer HBs.

The lower concentration predicted for GCs predominantly composed of FG stars seems well matched by the clusters probably belonging to Sgr, which tend to show a lower concentration (see the Harris 1996 catalogue).

Finally, a larger binary fraction should be found among FG stars than in SG stars, as we proposed in D'Orazi et al. (2010). This again stems from the different concentrations of the two populations; the SG binaries are more susceptible to beying destroyed by collisions. We used the binary fractions measured by Milone et al. (2012b) and found that Arp 2, NGC 4590, NGC 5053, Pal 12, Ter 7, and Ter 8 seem to have binary fractions larger than the majority of MW GCs, from more than 10% up to 20%, compared to <5% (see Fig. 9, where three different

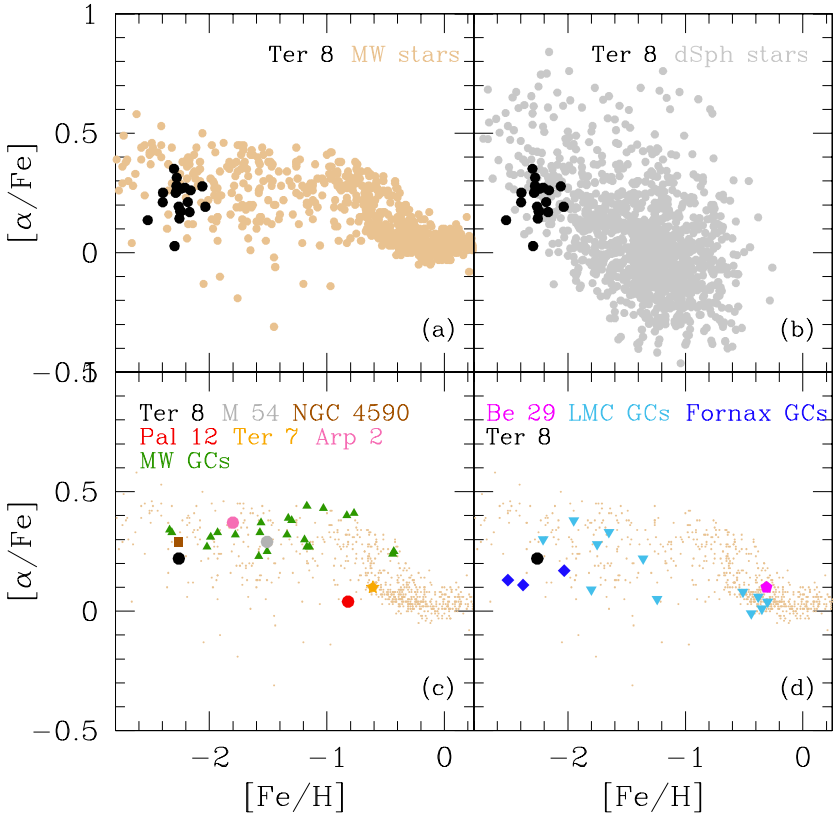

Fig. 10. Ratio [α/Fe] versus metallicity in several Galactic and extragalactic stellar populations. In **a)** the ratios for individual stars analysed in Ter 8 (large black circles) are superimposed on stars in our Galaxy from the compilation by Venn et al. (2004; brown circles). In **b)** the individual values for Ter 8 are superimposed on those for stars in eight dwarf galaxies from the extensive study by Kirby et al. (2010; grey circles). The average [α/Fe] ratio for Ter 8 (black circle) is compared in panel **c)** to the average ratios of GCs associated with Sgr (M 54, grey circle; NGC 4590, brown square; Arp 2, magenta circle; Ter 7, orange star; Pal 12, red circle) and to the mean ratios for MW GCs (green triangles). Finally, in **d)** the average value for Ter 8 is compared to several extragalactic clusters: GCs in the Fornax dwarf galaxy (blue diamonds), clusters in LMC (cyan triangles), and Be 29, an open cluster associated with Sgr. As a comparison, the small brown dots in panels **c)** and **d)** indicate the field stars in the Galaxy from Venn et al. (2004).

regions from Milone et al. 2012b are considered). Admittedly, this is more a hint than a firm conclusion, given the spread of the relations and the fact that lower mass GCs tend to have larger binary fractions. However, among GCs of similar mass, the clusters associated with the Sgr galaxy seem to show a tendency for higher binary fractions (especially in the lower panel of the figure).

In summary, it is possible to identify some common features in GCs formed in and/or presently residing in dwarf galaxies (especially in dwarf spheroidals). They tend to be less concentrated and more dominated by FG stars, unlike those of the inner halo of the MW. To these signatures we can also add that the escape velocity is usually low in these objects.

An interesting possible example of this process caught in the act is the double cluster NGC 1850a+b in the LMC (Gilmozzi et al. 1994). The younger component, NGC 1850b, should correspond to the SG in the framework depicted above, and is much smaller (about 10^3 $M_\odot$) than the 10^5 $M_\odot$ mass of NGC 1850a, which should represent the older, FG component. Unless there is an unknown mechanism producing selective mass loss in the latter, the FG will dominate even after the merging of the two components.

5.3. α- and heavier elements

The pattern of abundances of α-elements found in the stars in Ter 8 bears the typical signature of nucleosynthesis from massive stars only. In panels (a) and (b) in Fig. 10, values of the [α/Fe] ratio (the average of Mg, Si, Ca, and Ti I abundances) for individual stars in Ter 8 are superimposed on the values for Galactic field stars (from the compilation by Venn et al. 2004) and giants in eight dSph galaxies (Kirby et al. 2010). Our sample is compatible with the overabundance of α−elements also shown by the comparison samples of the MW and dSph stars at similar metallicities, suggesting an insignificant contribution from type Ia SNe to the nucleosynthesis.

The average [α/Fe] ratio for Ter 8 is compared in panel (c) of Fig. 10 to the average values for other GCs in the Galaxy, and in panel (d) to extragalactic GCs. The mean abundance in Ter 8 agrees well with that of other Galactic GCs, and with that of metal-poor GCs associated with the Sgr dSph (NGC 4590, M 54, Arp 2). On the other hand, the level of α-elements in stars of the more metal-rich GCs of Sgr (Pal 12 and Ter 7) is distinctly lower, and very evident if compared to the Galactic field stars (Venn et al. 2004, ad references therein).

The abundance of Mn (an element related to the neutron excess and, as a consequence, to the metal abundance) in Ter 8 perfectly agrees with those of Galactic field stars of similar metallicities (Fig. 11, panel (a)). The GCs in the MW and in Sgr also follow closely the trend of [Mn/Fe] as a function of metal abundance displayed by field stars in the Galaxy; the trend mirrors the pattern of the α-elements.

Abundances of the light neutron-capture element yttrium and of the heavy neutron-capture element barium are plotted in

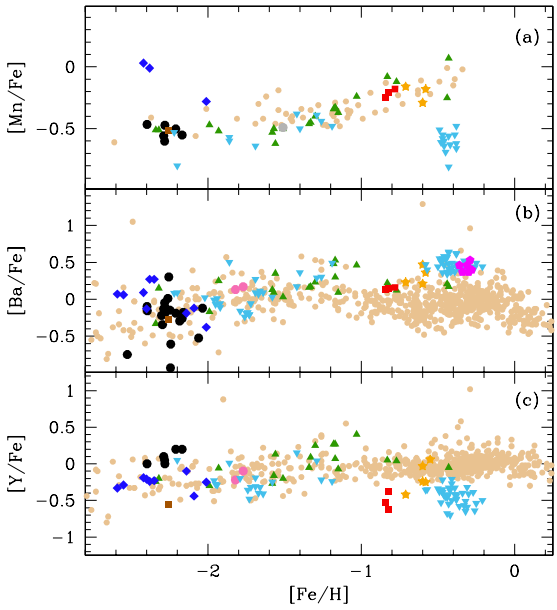

Fig. 11. As in the previous figure, but for the heavier elements Mn, Ba, and Y. In this case we give average values for the MW GCs and individual abundance ratios for the other clusters. Abundances of Mn for Galactic field stars are from Gratton et al. (2003).

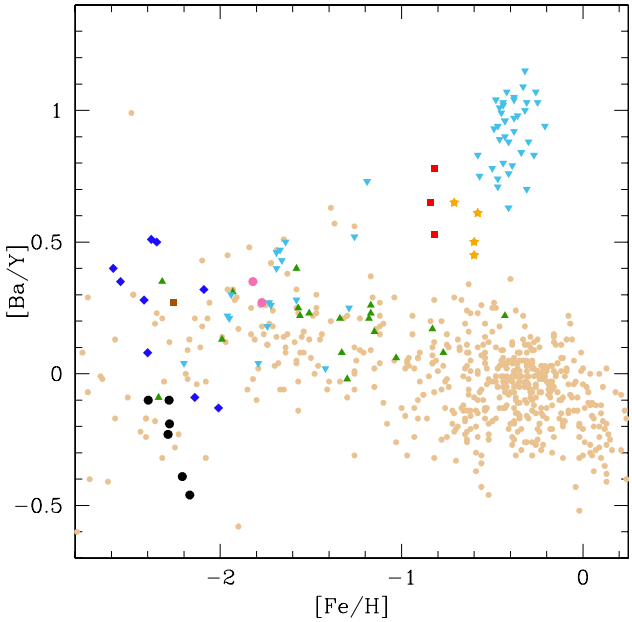

Fig. 12. Abundance ratios [Ba/Y] as a function of the metallicity. Symbols are as in the previous figure.

panels (b) and (c) of Fig. 11, and their ratio is plotted in Fig. 12 as a function of the metallicity. This ratio is important because Y and Ba sample different peaks in the production of *s*-process elements; Y belongs to the first peak around neutron magic number $N = 50$, whereas Ba belongs to the second peak that is built around $N = 82$. The ratio [*hs*/*ls*] of heavy-to-light *s*-process elements is useful for probing the efficiency of the neutron-capture process. For low efficiency, the neutron flux mainly feeds the first peak nuclei, whereas the species in the second peak (like Ba) are favoured in the case of higher neutron exposures (higher efficiency; see Busso et al. 2001). The Ba lines are not the best indicators, because they are generally strong, with limited sensitivities to changes in the abundances. A better candidate would be La that has a similar nucleosynthetic history and *s*-process contribution to the abundances in the solar system. Unfortunately, the La lines are too weak to be detected in our spectra of Ter 8.

The [Ba/Y] ratio of the most metal-rich GCs associated with Sgr (Pal 12 and Ter 7) is large, about 0.5 dex, much higher than the bulk of Galactic field stars of similar metallicity. This is also true for the metal-rich Sgr stars (see Sbordone et al. 2007 and Smecker-Hane & McWilliam 2002). As discussed in the latter paper, the ratio [La/Y] = 0.45 dex could indicate a significant contribution of metal-poor AGB stars: at low metallicity, the efficiency of the third dredge-up increases, as well as the number of available neutrons, simultaneosly with the decrease of seed nuclei. These occurrences shift the bulk of *s*-process production toward heavier elements in the second peak, so that the ratio [Ba/Y] (or [La/Y]) is high. Our data in Ter 8 do not present this evidence, although the sample is too small to draw any firm conclusions.

6. Summary

We have observed Ter 8, which belongs to the Sgr dSph family, using VLT/FLAMES with the intent of detecting a Na-O anticorrelation in this low-mass GC. From the spectra of six stars observed with UVES and 10 with GIRAFFE, we have measured Fe, Na, and O abundances (the last only in the UVES spectra). We did not detect any O underabundance, and we found only one star that shows an enhanced value of Na.

In Ter 8 we found one star with the typical chemical composition of SG stars. In this case, these stars represent a minority fraction, i.e. about 6% of the population, the opposite of what is found for higher mass MW clusters (Carretta et al. 2010), and also at variance with other low-mass Sgr GCs, Pal 12 a and Ter 7, where no significant Na and O spread was seen. Ter 8 may represent a candidate for the class of mainly-FG cluster, while the two other GCs can be considered as good candidates for FG-only clusters (Caloi & D'Antona 2011), with the caveat that only a very few stars were analysed in the last two clusters.

Not all Sgr dSph GCs studied present the same situation; a dichotomy exists between the metal-poor, (very) high-mass M54 (and maybe NGC 4590) and the low-mass GCs. We compared the case of Ter 8 to the clusters in Fornax and LMC showing variations in Na and O. The environment where the clusters formed (i.e. a dwarf galaxy) combines with cluster mass to define whether they could retain a large fraction of the original population, hence showing a dominance of FG over SG. Further studies of low-mass clusters in the MW and in neighbouring galaxies are required to disentangle the effects and better constrain cluster formation mechanisms. In particular, it would be interesting to target clusters that have a higher probability of having been formed in dwarf galaxies and later accreted by the MW. They should preferentially reside in the outer halo, could be younger, might display peculiarities in their variables and generally should show the features discussed above.

Acknowledgements. V.D. is an ARC Super Science Fellow. This publication makes use of data products from the Two Micron All Sky Survey, which is a joint project of the University of Massachusetts and the Infrared Processing and Analysis Center/California Institute of Technology, funded by the National Aeronautics and Space Administration and the National Science Foundation. This research has been funded by PRIN INAF 2011 "Multiple populations in globular clusters: their role in the Galaxy assembly" (PI E. Carretta), and PRIN MIUR 2010-2011, project "The Chemical and Dynamical Evolution of the Milky Way and Local Group Galaxies" (PI F. Matteucci). We made use of the package CataPack, for which we are grateful to Paolo Montegriffo. We thank Emanuele Dalessandro for his help with the GALEX data. This research has made use of the WEBDA, the SIMBAD database, operated at the CDS, Strasbourg, France, and of NASA's Astrophysical Data System.

References

Alonso, A., Arribas, S., & Martinez-Roger, C. 1999, A&AS, 140, 261
Alonso, A., Arribas, S., & Martinez-Roger, C. 2001, A&A, 376, 1039
Bekki, K. 2011, MNRAS, 412, 2241
Bragaglia, A., Carretta, E., Gratton, R. G., et al. 2001, AJ, 121, 327
Bragaglia, A., Gratton, R. G., Carretta, E., et al. 2012, A&A, 548, A122
Busso, M., Gallino, R., Lambert, D. L., Travaglio, C., & Smith, V. V. 2001, ApJ, 557, 802
Caloi, V., & D'Antona, F. 2011, MNRAS, 417, 228
Carretta, E. 2013, A&A, 557, A128
Carretta, E., Bragaglia, A., Gratton R. G., et al. 2006, A&A, 450, 523
Carretta, E., Bragaglia, A., Gratton, R. G., et al. 2009a, A&A, 505, 117
Carretta, E., Bragaglia, A., Gratton, R. G., & Lucatello, S. 2009b, A&A, 505, 139
Carretta, E., Bragaglia, A., Gratton, R.G., D'Orazi, V., & Lucatello, S. 2009c, A&A, 508, 695
Carretta, E., Bragaglia, A., Gratton, R. G., et al. 2010a, A&A, 516, A55
Carretta, E., Bragaglia, A., Gratton, R. G., et al. 2010b, ApJ, 714, L11
Carretta, E., Bragaglia, A., Gratton, R. G., et al. 2010c, A&A, 520, A95
Carretta, E., Lucatello, S., Gratton, R. G., Bragaglia, A., & D'Orazi, V. 2011a, A&A, 533, A69
Carretta, E., Bragaglia, A., Gratton, R., D'Orazi, V., & Lucatello, S. 2011b, A&A, 535, A121
Carretta, E., Bragaglia, A., Gratton, R. G., et al. 2013, A&A, 557, A138
Cohen, J. G. 2004, AJ, 127, 1545
D'Antona, F., Caloi, V., D'Ercole, A., et al. 2013, MNRAS, 434, 1138
D'Ercole, A., Vesperini, E., D'Antona, F., McMillan, S. L W., & Recchi, S. 2008, MNRAS, 391, 825
D'Orazi, V., Gratton, R. G., Lucatello, S., et al. 2010, ApJ, 719, L213
Da Costa, G. S., & Armandroff, T. E. 1995, AJ, 109, 2533
Dalessandro, E., Schiavon, R. P., Rood, R. T., et al. 2012, AJ, 144, 126
Decressin, T., Baumgardt, H., Charbonnel, C., & Kroupa, P. 2010, A&A, 516, A73
Ferraro, F. R., Paltrinieri, B., Fusi Pecci, F., et al. 1997, A&A, 324, 915
Fusi Pecci, F., Ferraro, F. R., Corsi, C. E., Cacciari, C., & Buonanno, R. 1992, AJ, 104, 1831
Gilmozzi, R., Kinney, E. K., Ewald, S. P., Panagia, N., & Romaniello, M. 1994, ApJ, 435, L43
Gratton, R. G. 1988, Rome Obs. Preprint Ser., 29
Gratton, R. G., Carretta, E., Eriksson, K., & Gustafsson, B. 1999, A&A, 350, 955
Gratton, R. G., Bonifacio, P., Bragaglia, A., et al. 2001, A&A, 369, 87
Gratton, R. G., Carretta, E., Claudi, R., Lucatello, S., & Barbieri, M. 2003, A&A, 404, 187
Gratton, R. G., Sneden, C., & Carretta, E. 2004, ARA&A, 42, 385
Gratton, R. G., Carretta, E., Bragaglia, A., Lucatello, S., & D'Orazi, V. 2010, A&A, 517, A81
Gratton, R. G., Carretta, E., & Bragaglia, A. 2012, A&AR, 20, 50
Gratton, R. G., Lucatello, S., Sollima, et al. 2013, A&A, 549, A41
Harris, W. E. 1996, AJ, 112, 1487
Hill, V., François, P., Spite, M., Primas, F., & Spite, F. 2000, A&AS, 364, 19
Ibata, R. A., Gilmore, G., & Irwin, M. J. 1994, Nature, 370, 194
Ibata, R. A., Gilmore, G., & Irwin, M. J. 1995, MNRAS, 277, 781
Johnson, J. A., Ivans, I. I., & Stetson, P. B. 2006, ApJ, 640, 801
Kirby, E. N., Guhathakurta, P., Simon, J. D., et al. 2010, ApJS, 191, 352
Kraft, R. P. 1994, PASP, 106, 553
Kurucz, R. L. 1993, ATLAS9 Stellar atmosphere programs and 2 km s^{-1} grid, CD-ROM 13 (Cambridge, MA: Smithsonian Astrophys. Obs.)
Law, D. R., & Majewski, S. R. 2010, ApJ, 718, 1128
Lee, J.-W., Kang, Y.-W., Lee, J., & Lee, Y.-W. 2009, Nature, 462, 480
Letarte, B., Hill, V., Jablonka, P., et al. 2006, A&A, 453, 547
Magain, P. 1984, A&A, 134, 189
McWilliam, A., Wallerstein, G., & Mottini, M. 2013, ApJ, 778, 149
Milone, A. P., Piotto, G., Bedin, L. R., et al. 2012a, ApJ, 744, 58
Milone, A. P., Piotto, G., Bedin, L. R., et al. 2012b, A&A, 540, A16
Milone, A. P., Marino, A. F., Piotto, G., et al. 2013, ApJ, 767, 120
Montegriffo, P., Bellazzini, M., Ferraro, F. R., et al. 1998, MNRAS, 294, 315
Mottini, M., Wallerstein, G., & McWilliam, A. 2008, AJ, 136, 614
Mucciarelli, A., Carretta, E., Origlia, L., & Ferraro, F. R. 2008, AJ, 136, 375
Mucciarelli, A., Origlia, L., Ferraro, F. R., & Pancino, E. 2009, ApJ, 695, L134
Pasquini, L., Avila, G., Blecha, A., et al. 2002, The Messenger, 110, 1
Piotto, G., Milone, A. P., Anderson, J., et al. 2012, ApJ, 760, 39
Renzini, A., & Fusi Pecci, F. 1988, ARA&A, 26, 199
Salinas, R., Catelan, M., Smith, H. A., Pritzl, B. J., & Borissova, J. 2005, Information Bulletin on Variable Stars, 5640, 1
Salinas, R., Jílková, L., Carraro, G., Catelan, M., & Amigo, P. 2012, MNRAS, 421, 960
Sbordone, L., Bonifacio, P., Buonanno, R., et al. 2007, A&A, 465, 815 (S07)
Sbordone, L., Salaris, M., Weiss, A., & Cassisi, S. 2011, A&A, 534, A9
Schiavon, R. P., Dalessandro, E., Sohn, S. T., et al. 2012, AJ, 143, 121
Skrutskie, M. F., Cutri, R. M., Stiening, R., et al. 2006, AJ, 131, 1163
Smecker-Hane, T. A., & McWilliam, A. 2002, unpublished [arXiv:astro-ph/0205411]
Tautvaišienė, G., Wallerstein, G., Geisler, D., Gonzalez, G., & Charbonnel, C. 2004, AJ, 127, 373
van den Bergh, S., & Mackey, A. D. 2004, MNRAS, 354, 713
Venn, K. A., Irwin, M., Shetrone, M. D., et al. 2004, AJ, 128, 1177
Vesperini, E., McMillan, S. L. W., D'Antona, F., & D'Ercole, A. 2013, MNRAS, 429, 1913
Villanova, S., Geisler, D., Carraro, G., Moni Bidin, C., Munoz, C. 2013, ApJ, 778, 186
Webbink, R. F. 1985, in Proc. Dynamic of star clusters, IAU Symp., 113, 541
Worley, C. C., Hill, V., Sobeck, J., & Carretta, E. 2013, A&A, 553, A47
Yong, D., Grundahl, F., Nissen, P. E., Jensen, H. R., & Lambert, D. L. 2005, A&A, 438, 875

Pages 14 to 16 are available in the electronic edition of the journal at http://www.aanda.org

Table 2. Information on the stars observed in Ter 8.

ID	RA (hh mm ss)	Dec (dd pp ss)	V	I	K (2MASS)	RV (km s^{-1})	err.	Notes
2357	19 42 00.02	–33 58 21.52	15.072	13.570	11.697	144.64	0.52	UVES
1658	19 41 49.77	–33 59 44.53	15.269	13.838	12.033	146.07	0.39	UVES
530	19 41 55.64	–34 01 48.12	15.288	13.881	12.114	144.17	0.53	UVES
1188	19 41 37.06	–34 00 33.78	15.411	14.069	12.304	145.65	0.66	UVES
3014	19 41 23.69	–33 56 03.30	15.447	14.082	12.218	0.75	0.52	UVES,NM

Notes. The complete table is available electronically only at the CDS.

Table 3. Adopted atmospheric parameters and derived iron abundances.

Star	$T_{\rm eff}$ (K)	log g (dex)	[A/H] (dex)	$v_{\rm t}$ (km s^{-1})	n	[Fe/H]I (dex)	rms	No.	[Fe/HII (dex)	rms
1209	4264	0.80	−2.16	2.14	20	−2.160	0.092	1	−2.066	
1169	4567	1.38	−2.25	1.96	17	−2.248	0.168			
2086	4547	1.33	−2.30	1.98	13	−2.301	0.147	2	−2.218	0.292
526	4589	1.42	−2.40	1.95	13	−2.395	0.128	1	−2.328	
1728	4604	1.45	−2.24	1.94	17	−2.242	0.120			
2913	4628	1.49	−2.52	1.93	10	−2.525	0.067			
514	4635	1.50	−2.19	1.93	17	−2.184	0.139	1	−2.240	
496	4660	1.54	−2.04	1.91	17	−2.035	0.158			
126	4777	1.79	−2.26	1.84	13	−2.261	0.134			
2124	4730	1.67	−2.28	1.87	18	−2.278	0.256	1	−2.271	
1077	4741	1.70	−2.06	1.86	11	−2.060	0.071			
2531	4762	1.74	−2.24	1.85	12	−2.244	0.151			
2180	4783	1.79	−2.25	1.84	14	−2.255	0.224			
2023	4793	1.81	−2.30	1.83	8	−2.296	0.115			
2357	4188	0.66	−2.29	2.18	52	−2.288	0.100	13	−2.302	0.157
1658	4264	0.80	−2.39	2.14	28	−2.397	0.073	11	−2.400	0.132
530	4282	0.84	−2.28	2.13	50	−2.280	0.108	13	−2.293	0.092
1188	4325	0.92	−2.28	2.10	32	−2.282	0.112	11	−2.264	0.117
2253	4442	1.14	−2.17	2.04	51	−2.168	0.117	14	−2.152	0.128
137	4472	1.19	−2.21	2.02	45	−2.209	0.116	10	−2.226	0.106

Table 7. Abundances of proton-capture elements in Ter 8 stars.

Star	n	[O/Fe]	rms	n	[Na/Fe]	rms	n	[Mg/Fe]	rms	n	[Al/Fe]	rms	limNa	limAl
1209				2	+0.14	0.10	1	0.48					1	
1169				1	+0.05		1	0.37					0	
2086				2	+0.24	0.11	1	0.50					1	
526				1	−0.10								1	
1728				2	+0.33	0.07	1	0.36					0	
2913							1	0.58						
514							1	0.43						
496				1	+0.10		1	0.36					1	
126				1	+0.10		1	0.47					1	
2124				1	+0.13		1	0.56					0	
1077				1	−0.06								1	
2531							1	0.50						
2180														
2023				2	+0.88	0.01							1	
2357	1	+0.44		3	+0.29	0.11	2	0.48	0.14	1	+0.84		1	0
1658	1	+0.40		3	+0.19	0.04	2	0.51	0.02	1	+0.77		1	0
530	1	+0.31		3	+0.25	0.07	2	0.60	0.26	1	+0.85		1	0
1188	1	+0.42		3	+0.50	0.19	2	0.50	0.26	1	+1.27		1	0
2253	1	+0.40		3	+0.15	0.14	2	0.33	0.21	1	+0.94		1	0
137	1	+0.40		3	+0.14	0.07	2	0.40	0.16	1	+1.09		1	0

Notes. n is the number of lines used in the analysis. Upper limits (limNa, Al=0) and detections (=1) in Na and Al are flagged.

Table 8. Abundances of α-elements in Ter 8 stars.

Star	n	[Si/Fe]	rms	n	[Ca/Fe]	rms	n	[Ti/Fe] I	rms	n	[Ti/Fe] II	rms
1209	2	+0.35	0.04	6	+0.21	0.22	4	+0.00	0.16			
1169				5	+0.19	0.23	1	+0.14				
2086	3	+0.55	0.03	4	+0.21	0.04	2	+0.16	0.24			
526	2	+0.54	0.05	4	+0.33	0.24	2	+0.13	0.08			
1728	2	+0.42	0.06	5	+0.24	0.30	1	+0.06				
2913				2	−0.03	0.15						
514				3	+0.19	0.26	2	+0.23	0.06			
496	3	+0.28	0.33	4	+0.21	0.13	1	−0.09				
126				4	+0.18	0.17	1	+0.12				
2124	3	+0.44	0.29	3	+0.26	0.20						
1077	2	+0.40	0.10	4	+0.35	0.28	2	+0.37	0.08			
2531				4	+0.08	0.03	3	+0.12				
2180	1	+0.44		3	+0.13	0.13	1	+0.01				
2023				3	+0.11	0.24						
2357	1	+0.25		18	+0.21	0.15	19	+0.07	0.11	6	+0.11	0.17
1658	1	+0.24		15	+0.15	0.09	16	−0.06	0.09	5	+0.18	0.14
530	2	+0.24	0.11	18	+0.22	0.11	18	+0.06	0.07	7	+0.16	0.11
1188	1	+0.32		13	+0.13	0.15	13	+0.06	0.15	6	+0.15	0.16
2253	1	+0.08		19	+0.22	0.12	17	+0.05	0.15	6	−0.01	0.12
137	1	+0.35		15	+0.22	0.15	11	+0.12	0.09	5	+0.12	0.09

Notes. n is the number of lines used in the analysis.

Table 9. Abundances of Fe-peak elements in Ter 8 stars.

Star	n	[Sc/Fe] II	rms	n	[V/Fe]	rms	n	[Cr/Fe] I	rms	n	[Mn/Fe]	rms	n	[Ni/Fe]	rms	n	[Cu/Fe]	rms	n	[Zn/Fe]	rms
1209	7	−0.07	0.11	5	−0.11	0.22	1	−0.15					5	−0.05	0.10						
1169	7	−0.09	0.11	2	+0.00	0.13	1	−0.03					2	−0.05	0.10						
2086	5	−0.11	0.14	1	+0.04								3	+0.03	0.31						
526	5	+0.00	0.11	3	+0.07	0.11							2	+0.05	0.46						
1728	6	−0.08	0.35	2	+0.10	0.02							1	−0.04							
2913					99								2	+0.21	0.02						
514	5	+0.10	0.31	1	+0.13								1	−0.04							
496	7	+0.02	0.16	2	−0.11	0.09	1	−0.18					3	−0.05	0.14						
126	4	+0.06	0.19		99								1	−0.04							
2124	6	+0.05	0.29		99								2	−0.01	0.14						
1077	4	−0.12	0.20	2	−0.12	0.29							1	−0.01							
2531	2	+0.06	0.11	1	+0.06								1	−0.14							
2180	3	−0.01	0.15	1	+0.03								2	+0.04	0.28						
2023	4	+0.13	0.14		99								1	−0.00							
2357	7	−0.09	0.08	4	−0.35	0.08	8	−0.47	0.10	5	−0.56	0.21	12	−0.17	0.10	1	−0.55		1	−0.02	
1658	7	−0.13	0.11	5	−0.23	0.15	7	−0.42	0.08	5	−0.47	0.14	4	−0.13	0.22	1	−0.55		1	−0.05	
530	8	−0.11	0.09	4	−0.30	0.09	7	−0.36	0.12	4	−0.47	0.17	8	−0.17	0.13	1	−0.75		1	−0.15	
1188	5	−0.11	0.05	3	−0.39	0.20	7	−0.47	0.11	3	−0.60	0.24	5	−0.21	0.17	1	−0.59		1	+0.09	
2253	7	−0.21	0.12	2	−0.27	0.04	7	−0.38	0.14	5	−0.55	0.15	12	−0.20	0.16	1	−0.60		1	−0.12	
137	5	−0.07	0.04	1	−0.26		7	−0.35	0.17	2	−0.50	0.01	4	−0.18	0.04	1	−0.65		1	−0.04	

Notes. n is the number of lines used in the analysis.

Table 10. Abundances of *n*-capture elements in Ter 8 stars with UVES spectra.

Star	*n*	[Y/Fe] II	rms	*n*	[Ba/Fe] II	rms	*n*	[Nd/Fe] II	rms	*n*	[Eu/Fe] II	rms
2357	1	0.10		3	−0.13	0.04	2	0.23	0.59	1	<2.39	
1658	1	0.00		3	−0.10	0.04	2	−0.25	0.12	1	<2.79	
530	1	0.00		3	−0.19	0.03	4	−0.55	0.12	1	<2.63	
1188	1	0.05		3	−0.05	0.06	3	−0.57	0.17	1	<2.70	
2253	1	0.20		3	−0.26	0.05	4	−0.52	0.12	1	<2.59	
137	1	0.20		3	−0.19	0.06	3	−0.12	0.23	1	<2.77	
1209				1	−0.18							
1169				1	−0.15							
2086				1	−0.22							
526				1	−0.16							
1728				1	−0.61							
2913				1	−0.75							
514				1	−0.30							
496				1	−0.12							
126				1	+0.01							
2124				1	−0.12							
1077				1	−0.53							
2531				1	−0.93							
2180				1	+0.30							
2023				1	−0.34							

Notes. *n* is the number of lines used in the analysis.